Batteries & Supercaps

Research Article
doi.org/10.1002/batt.202500133

Chemistry Europe
European Chemical Societies Publishing

www.batteries-supercaps.org

Analysis of Quality-Relevant Process–Structure Relationships through Tracking and Tracing: A Comprehensive Study on the Calendering Process in Lithium-Ion Battery Production

Andreas Mayr,* Alessandro Sommer,* Julian Link, Johannes Schachtl, and Rüdiger Daub

The calendering process represents the final step in the electrode manufacturing for lithium-ion batteries. This process significantly influences and adjusts electrochemical and mechanical parameters. The major challenges are the unknown cause-effect relationships as well as the high setup effort to reach desired electrode parameters. This article presents an innovative approach using an integrated marker-based traceability system to link machine and sensor data to key inline production parameters during electrode calendering. Offline measurements are generated after calendering, which are assigned to individual electrode sections via the applied markings. This allowed correlations to be derived between the set machine parameters, the measured inline data, and subsequently the measured offline data. Using a stepwise experimental plan, an electrode is calendered, and its compaction behavior is extensively characterized. From the determined relationships, the machine parameters to be adjusted for targeted electrode properties can be efficiently derived. The types of defects that occur with increasing calendering degree are quantified using the appropriate measurement technology and traced back to the set machine parameters. The implementation of this approach enables a substantial reduction in the setup effort required for the calendering process, necessitating a limited degree of experimental effort.

1. Introduction

Lithium-ion batteries (LIBs) play an important role in reducing greenhouse gases in the transportation sector. Due to their high energy and power density, they represent a suitable basis for electric drive technology compared to fossil-fueled engines.[1] However, LIB production is characterized by a complex and cost-intensive process chain.[2] Lowering the manufacturing costs, mainly driven by material expenses and high scrap rates, is crucial for the widespread acceptance of electric vehicles.[3,4] Optimizing electrode manufacturing processes and using innovative materials are key to reducing costs and improving LIB properties, such as the energy density.[5,6] LIB electrodes consist of active material particles, binders, and conductive additives that are coated onto a metallic substrate foil and have a porous microstructure.[7] The quality of the electrodes is largely dependent on the manufacturing processes employed, as these have a profound impact on electrode properties.[8] Research on a pilot scale is essential to enable an independent mass production of high-energy LIBs that meet the standards of the automotive industry.[9] On the process side, reducing scrap during startup and operation until the target electrode quality is achieved represents a key factor for cost reduction. Particularly on small production lines, the scrap rate during initial startup and the associated adjustment of process parameters is significant.[10]

Calendering represents the final property-determining process step during electrode manufacturing, with a significant and irreversible impact on the quality characteristics of the produced battery electrodes.[11] This process reduces the pore volume and increases the volumetric energy density of the electrodes by subjecting the material to compression between two rollers.[12] Accordingly controlling the associated microstructure and porosity of the electrodes is crucial for maximizing battery performance.[13] However, the pursuit of higher volumetric energy densities and associated elevated compaction rates increases electrode defects and scrap during calendering, impairing the quality-cost balance.[3] Therefore, it is important to efficiently design the calendering process to meet the high volumetric energy density and long lifespan requirements of LIBs while ensuring the efficiency and cost-effectiveness of production, particularly with regard to recurring switch-on processes.[2,10] The integration of innovative active materials to further improve energy density and electrochemical performance presents a challenge to the calendering process. This requires optimization of the process parameters at an early stage, often through trial and error, to achieve the desired electrode

A. Mayr, A. Sommer, J. Link, J. Schachtl, R. Daub
Technical University of Munich
TUM School of Engineering and Design
Institute for Machine Tools and Industrial Management (iwb)
Boltzmannstr. 15, 85748 Garching, Germany
E-mail: andreas.mayr@iwb.tum.de
alessandro.sommer@iwb.tum.de

R. Daub
Fraunhofer Institute for Casting, Composite and Processing Technology (IGCV)
Am Technologiezentrum 10, 86159 Augsburg, Germany

Supporting information for this article is available on the WWW under https://doi.org/10.1002/batt.202500133

quality.[14] It is therefore crucial to employ a holistic approach to the analysis of the interdependencies between machine and material parameters, as well as process and structural interactions, to achieve a well-parametrized calendering process.

2. State of the Art

The primary objective of calendering is to optimize process parameters to achieve high volumetric energy densities while balancing mechanical and electrochemical properties of the electrodes and guaranteeing economic viability.[3,15] These interdependencies require an understanding of the trade-offs inherent to the material properties. For instance, an elevated degree of porosity can improve ionic conductivity but simultaneously diminish electrical conductivity, while a higher compaction rate can enhance electrical conductivity while concurrently reducing ionic conductivity.[13,16] It has been demonstrated that the homogenization of the mechanical properties, particularly as a result of calendering, leads to enhanced cell performance and homogeneous aging behavior in LIBs.[17] Moreover, an improvement in the adhesion strength between the electrode coating and the metallic substrate foil, along with an increase in cohesion within the coating, is attributed to the calendering process.[11,13] The improved adhesion strength exhibited with increasing compaction in cathodes can be ascribed to the enhanced mechanical interlocking between the active material particles and the substrate foil, resulting from plastic deformation.[11,18] The enhancement of mechanical contact at the interface between the coating and the substrate foil has a considerable impact on the thermal conductivity of the electrodes, demonstrating a strong correlation with the adhesion strength.[19] In more recent work, simulation models are increasingly used to represent the interfacial thermal resistance during heat transfer[20] in addition to the identification of compaction parameters.[21] Furthermore, elevated roller temperatures facilitate enhanced adhesion strength, due to the temperature-dependent modification of binder properties.[22]

Research has demonstrated that the compaction resistance of cathodes is greater than that of anodes. This phenomenon can be attributed to the increased hardness of the active material particles, which necessitates higher line loads for effective compaction.[12] For this reason, cathodes in particular are often characterized by defect patterns and the particles can undergo plastic deformation as well as particle breakage.[3,23] Defect patterns can be classified into three principal categories: geometric, structural, and mechanical.[3] In previous research studies, the temperature of the calendering rollers was identified as a relevant influencing factor for improving the processing properties in the calendering process.[14,24] Furthermore, concepts have already been developed to counteract geometric defects with additional rollers or grippers.[25] It was shown that the processability of cathodes in the calendering process is positively influenced by the targeted addition of graphite additives in the coating composition. This results in a reduction in the intensity of geometric defect patterns and, consequently, a decrease in the scrap rate.[26] In addition to intrinsic material properties, the processability and the resulting structural properties of the electrodes are also influenced by the specific calendering machine behavior, which was summarized in previous studies in a qualitative machine/material–process–structure model.[11] The goal is to fine-tune these parameters to maximize the overall energy density while addressing the mentioned trade-offs and correlations. As a result, there is still a significant need for expertise in electrode densification by calendering.[12,15]

The determination of achieved quality and the reduction of adjustment effort for electrode production, respectively the calendering process, necessitates a combination of inline and offline analyses of quality-relevant electrode properties.[3,27] Furthermore, the interlinked process steps and associated interdependencies require precise coordination of the quality-determining process and product parameters during the manufacturing process.[3] In previous studies, inline measuring systems were integrated into the calendering process to analyze specific defect patterns. For instance, electrode corrugation[24] and the formation of longitudinal wrinkles[28,29] were examined using laser triangulation sensors. In other instances, the relationship between the electrode corrugation after calendering and subsequent electrode singulation was analyzed.[30] Inline sensors can also be utilized for direct roll gap measurement to study the springback effect, providing real-time data that helps to understand the relationship between the compaction process, the machine performance, and the electrode structure.[31] To develop a comprehensive understanding of the calendering process for a specific material system, the use of a traceability system is therefore suggested.[32] This system enables efficient correlation analysis across multiple process steps, thereby facilitating the identification of quality-relevant process–structure relationships for individual process steps, for example, calendering.[33]

As indicated by the literature, a holistic approach to identifying cause-and-effect relationships and generating process understanding based on the tracking and tracing principle has yet to be implemented in existing research. A database that is consistently updated based on tracking and tracing information can also be used to develop data-based models. For example, artificial intelligence can be employed as a potential method for identifying interdependencies in electrode production.[34,35]

This work addresses the consistent linking of both inline and offline data through the utilization of tracking and tracing, thereby facilitating the characterization of the calendering process within a material- and machine-specific context. The goal of this article is to deepen the understanding of the calendering process by systematically identifying quality-relevant process–structure relationships. The calendering process is utilized as a case study in demonstrating the reliability of the traceability system, given its substantial dependency on the parameters of the incoming material and its considerable influence on the subsequent processing of the electrodes. To realize this approach, the present work implemented the recording of quality-relevant electrode properties using suitable inline sensors, existing offline quality measures, and a traceability system for consistent data allocation.

3. Experimental Section

3.1. Approach

The aim of this study was to provide a comprehensive description of the compaction behavior and its effects on the product properties of an electrode, utilizing a marker-based traceability system. This was accomplished by integrating an existing tracking and tracing system with corresponding inline sensors and by employing a selection of analytical offline measures. A commercially procured electrode, which was subsequently marked with the integrated laser unit in the coating system of the *iwb*, was used to obtain specific electrode sections (ESs). Subsequently, the electrode was calendered using stepwise compaction, and the inline measurement data was assigned to the specific ESs. After calendering, offline measurements of electrode thickness, porosity, particle indentations in the substrate foil, and adhesion strength were performed and associated with the corresponding sections of the electrode. The linkage of the offline measurement data with the applied inline production parameters was done via data matrix code (DMC) markings on the substrate foil of the electrode.

In the initial phase of this research, a process-specific real-time dashboard was developed to visualize the data generated during the process. This approach allows for the targeted identification of local anomalies in the process and the product. The data generated during the process is used by the traceability system to evaluate the process performance. The accurate allocation of data between inline and offline data facilitates the identification of correlation patterns and the proposal of appropriate measures for enhancing the efficiency of process operation. The following sections presented an overview of the sensors and peripherals utilized in the calendering system, a detailed examination of the underlying traceability concept employed in the *iwb* pilot line, a comprehensive analysis of the electrode composition, and a detailed description of the experimental procedures and offline measurements conducted.

3.2. Sensors and Infrastructure

The calendering system (EA 102, Coatema GmbH, Germany), which is available at the *iwb* production line and has been previously described in detail in previous publications,[11,14,24] was used to compact the electrode. The present study concentrated on the implementation of inline measurements for the purposes of detecting electrode corrugation, determining the actual roll gap, and acquiring calendering process data. All process parameters set by the operator were continuously recorded and stored in a central database. These included, for example, web speed, web tension, and roll temperature. The roll gap measurement was conducted using four capacitive measuring sensors (CSH2FL-CRm1.4, Micro-Epsilon, Germany). This approach enabled the detection of the displacement of the upper and lower roller and consequently facilitated the calculation of the resulting roll gap value on both sides of the rollers. As previously described by Schreiner et al.,[21] the sensors were integrated into the existing calendering framework at *iwb*. A comparable system was used by Diener et al.[31] to analyze the springback behavior of cathodes in the calendering process. The electrode corrugation was measured using a laser triangulation sensor (LJ-X8400/LJ-X8000, Keyence, Japan), as was done previously by Mayr et al.[24]

The sensors described and the corresponding recorded process data were integrated into a real-time dashboard. This enables the synchronization with a central database and the integration of collected process data into the traceability system. Additionally, the dashboard supports the system operator in process monitoring and parameter setting. The overview page of the dashboard offered a comprehensive display of pertinent sensor, system, and process parameters, facilitating a uniform presentation of data essential for the calendering system's operational monitoring. The underlying functions of the communication units, including data acquisition, data identification, data translation, and data backup, were implemented using Python scripts. The process-specific dashboard visualization was developed using Node-RED.

The entire periphery, consisting of inline and offline measurements, is shown in **Figure 1**. The dashboard and the individual DMCs represented the central linking point.

3.3. Traceability System and Data Strategy

The continuous processes of electrode manufacturing were so far been considered only in batches.[36] This meant that the recorded production data were assigned to an entire electrode coil and not to individual sections. Integrated DMC markings made discrete ESs visible and could be used for traceability applications.[32,37] These DMCs were applied to the electrode current collectors of the substrate foil and read by scanners at key points in the production process.[38] This enabled data assignment down to individual ESs. For the investigations in this work, a scanner (DM280, Cognex, USA) was located after the roll gap of the calendering machine. This scanner identified marked ESs and made them available to the traceability system. The scanner was part of a comprehensive traceability system that was put into operation at the *iwb* pilot line.[33] In this work, offline measurement data was generated in addition to the inline recorded production data. The samples for the offline measurements were taken directly at the electrode markings and subsequently assigned to the corresponding code in the database. The code content thus allowed direct linking of the inline data with the offline data. Prior to calendering, the electrode coil was marked in the coating system (BC50, Coatema GmbH, Germany) of the *iwb*. For this purpose, it was guided through the coating system at a web speed of 1 m min^{-1} and labeled with electrode markings using an integrated laser system.[39] A unique DMC was applied every 100 mm, encoding a numbering starting at 1 for a new electrode coil and an abbreviation of the corresponding production batch. To mark the aluminum foil with a DMC of 5.6 × 5.6 mm, a traverse speed of 1500 mm s^{-1}, an intensity of 45%, and a pulse frequency of 10 kHz were chosen. Previous studies demonstrated that the marking of the

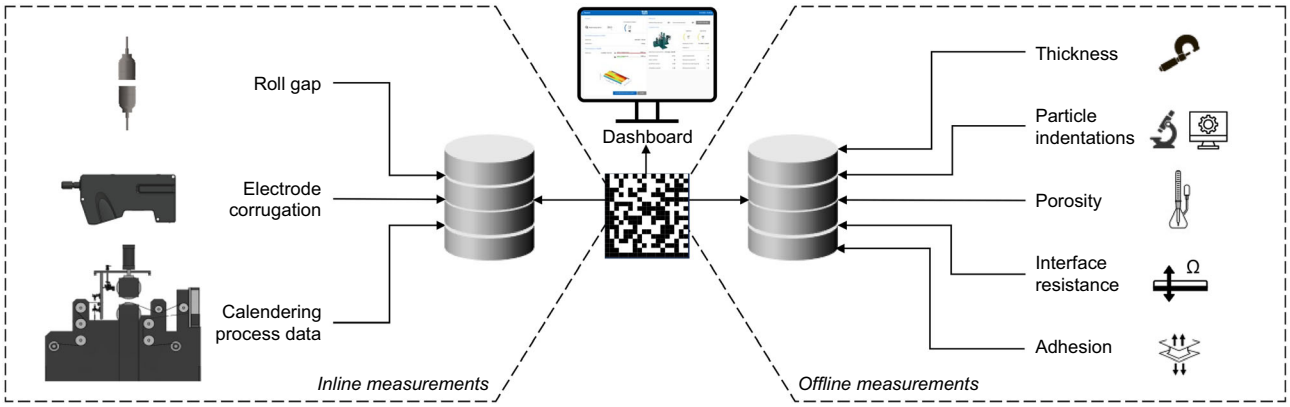

Figure 1. Periphery of the calendering setup for the investigations, divided into inline and offline measurements. The DMC marking on the individual ESs forms the interface between the two measurement data areas and allows the data to be linked consistently.

substrate foil resulted in a reduction in the mechanical strength of the material. However, this did not affect its processability.[38] In addition to the DMC, the unique number was displayed in Arabic characters on the current collector. This provided visual guidance on the electrode to assist the operator. The applied markings were used to establish defined experimental areas.

3.4. Materials, Procedure, and Analysis

For all investigations, a commercially procured state-of-the-art lithium nickel manganese cobalt oxide (NMC622) cathode (UniverCell GmbH, Germany) was used as a material system due to representativity application. Detailed information about the double-sided electrode is given in **Table 1**.

After marking in the coating system, the electrode was compacted in the calendering machine at ambient temperature. The web tension was set to 15 N. First, the respective rolling force was set to 350 kN and the web speed to 1 m min^{-1}. By adjusting the rolling force on the hydraulic cylinders of the calendering machine, different levels of compaction could be achieved, and the resulting roll gap could be varied. After ≈8 m, the target force was progressively decreased by around 50 kN per iteration, thereby establishing a total of six distinct compaction stages. During the final reduction to the 100 kN compaction stage, a rolling force of ≈120 kN was achieved. The cause of the difference between target and actual values for this compaction stage was attributed to a malfunction in the pressure control valve or the pressure control unit. This was not an obstacle as the aim was to set distinct compaction stages, and the deviation was negligible. The roll gap was opened for the last section of the electrode coil to obtain a non calendered reference, which was indicated by the rolling force of 0 kN. However, the non calendered electrode was still measured both inline and offline as a reference.

Table 1. Characteristics of the commercially available double-sided cathode.

Attribute	Value
Active material	NMC622
Active material content	95.5 wt%
Conductive additives	3.0 wt%
Binder (polyvinylidene fluoride)	1.5 wt%
Substrate foil	15 μm, aluminum (alloy Al1100)
Foil width	180 mm
Coating width	150 mm
Areal mass loading (per side)	18.3 mg cm^{-2}

Each individual compaction stage was allocated to a specific ES, which was defined by grouping the DMCs and the associated rolling force of the calendering machine. For all offline measurements, three sample positions were defined across the electrode width at a single DMC, namely next to the DMC, in the middle of the electrode and opposite the DMC. **Figure 2**a illustrates the sections reached by grouping the DMCs, and Figure 2b shows the sample positions for the offline measurements at a given DMC.

As illustrated in Figure 1, the calendering process was characterized using five different offline measurements. The resulting thickness of the electrode was measured using a tactile dial gauge (40 EWRi, Mahr GmbH, Germany, measuring tolerance: ± 1 μm) on the different sample positions.

For the determination of the electrodes' porosity, a pycnometer (Ultrapyc 5000 Micro, Anton Paar GmbH, Austria) was used. 25 samples were taken from each ESs, with a diameter of 10.95 mm. The samples were placed vertically in the sample chamber to ensure optimal exposure to the working gas argon. The working pressure was set to 1310 mbar. Measurements were taken until a convergence criterion of 0.1% for three measurements was reached. The porosity was calculated from the difference between the skeletal volume, as determined by the gas pycnometer, and the total sample volume calculated using the measured thickness and diameter of the samples.

The interfacial resistance of the electrodes was measured using an electrode resistance measurement system (RM2610, HIOKI E.E. Corp., Japan). These measurements were carried out directly on the electrode without taking samples in the form of punchings. For each ES, the interfacial resistance was measured

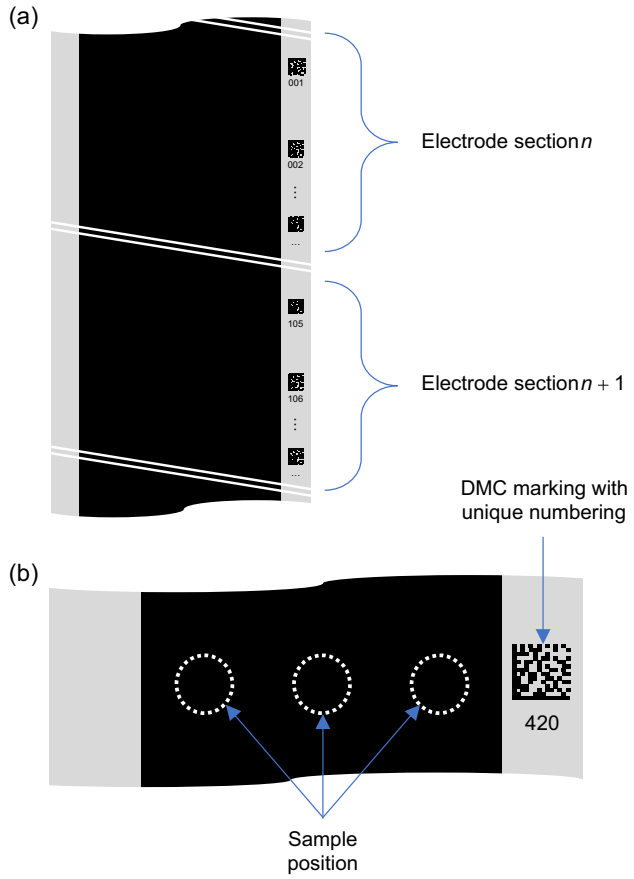

Figure 2. a) Schematic representation of the ESs by grouping several consecutive DMC labels. b) In addition, three measurement points were defined for sampling positions at a given DMC: next to the DMC, in the middle of the electrode, and opposite the DMC.

at three separate DMCs, and for each DMC, three measurements were carried out at each sample position, resulting in nine measured interfacial resistance values per ES.

The adhesion strength tests were conducted through a z-tensile test with a uniaxial material testing machine (Z020, ZwickRoell GmbH & Co.KG, Germany). Samples for adhesion testing were taken by punching at three specific DMCs for each ES at the three sample positions. The upper and lower sample holders with an area of 6.25 cm^2 were prepared with double-sided adhesive tape (#410 m, 3M, USA), and the cathode samples were placed on the lower holder. The testing procedure was adapted from Haselrieder et al.[40] A compression velocity of 0.75 mm min^{-1}, dwell time of 30 s, pull-off velocity of 100 mm min^{-1}, and data acquisition rate of 2000 Hz were used. The compression stress was set to 1000 kPa. Particularly in the case of highly calendered cathodes, the increased compression stress resulted in a higher and more homogeneous removal rate. The adhesion strength was defined to be the maximum tensile stress achieved at the point of adhesion failure.

For the measurement of the particle indentations in the aluminum substrate foil, samples were taken from three DMCs per ES. For each specific DMC, three die-cut samples were taken, analogous to the procedure described above for measuring the adhesion strength. The individual electrode samples were decoated using an ultrasonic bath. For this purpose, the electrode samples were immersed in glasses containing N-methyl-2-pyrrolidone (NMP) and left to soak for 24 h. The laboratory glasses containing the samples and the NMP were then subjected to an ultrasonic bath for around 10 min. Any remaining coating residues were wiped off the substrate foil with precision cleaning wipes. The decoated samples were examined using a laser scanning microscope (LSM) (VK-X1000, Keyence, Japan) at 50-fold magnification. The quantification of particle indentations represented a novel methodology for the characterization of alterations in microstructure that occurred at the interface between the substrate foil and coating particles as compression levels increased. An existing algorithm for analyzing the topographical data from the LSM was used to quantify the number of contact points between the substrate foil and the coating matrix.[41] The implementation of the automated geometry determination and the transfer of this approach to calendering was described in detail by Hille et al.[41] in a previous publication.

As outlined above, the inline measurements consisted of the calendering machine data as well as the additionally integrated sensor data. For the quantitative determination of the electrode corrugation, the defect evaluation index (DEI) was used. The DEI was shown to serve as a significant indicator for establishing a quantitative link between corrugations and process parameters during calendering. It also facilitated the identification of process–structure interactions, which are essential for the development of process knowledge.[24,30] The DEI was determined by calculating the difference in magnitude between the highest peak and the lowest valley of the corrugation signal detected in the deformed electrode.[24] The laser triangulation sensor was operated with a measuring frequency of around 222.2 Hz. For a single height image, a total of 10,000 profile lines were recorded in machine direction, covering the full width of the electrode, at a resolution of 75 μm, giving a total length of 750 mm. The resulting images were stored as bitmap files for subsequent postprocessing and analysis. The height data was encoded in the red, green, and blue values of the bitmap files, which were processed and displayed graphically to analyze the electrode corrugation. To obtain representative results for the electrode corrugation, each image was sampled along three profile lines. For every height image, the three profile lines extended over the entire electrode length of 750 mm and were located 40 mm from each side of the electrode width and in the middle of the electrode. The positioning of the profile lines for the calculation of the three DEI values therefore corresponds to the sample positions used for the offline measurements. **Figure 3** provides a visual representation of a height image and the corresponding profile lines for the DEI calculation.

The positioning of the three profile lines was selected due to the curvature present along the electrode width, which could result in smaller DEI values at the edge of the electrode compared to the center. For each line, the maximum and minimum values were determined to calculate the DEI, thus yielding three values for each image. For each ES, ≈10 images were analyzed, as each ES covered an electrode length of ≈8 m.

Research Article
doi.org/10.1002/batt.202500133
Chemistry Europe
European Chemical Societies Publishing

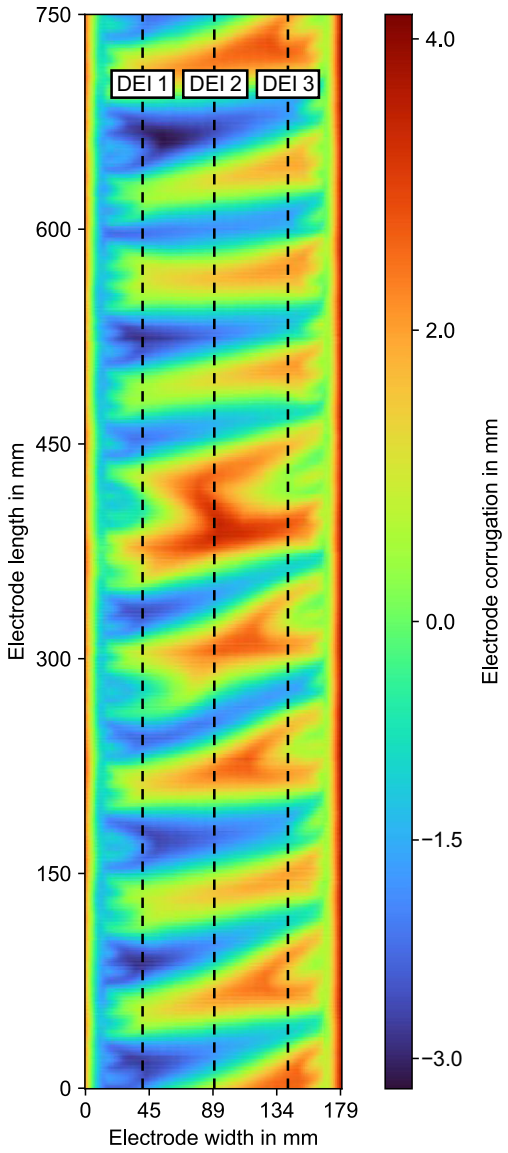

Figure 3. Depiction of a representative height image of the inline measurement of the electrode corrugation using laser triangulation. For each height image, three specific DEI values were determined along the profile lines (DEI 1–3).

4. Results and Discussion

The results chapter is divided into two sections. The initial section discusses the ESs generated by the varying compaction levels, whereas the subsequent section presents the results of the product properties that are dependent on the specified calendering degree.

4.1. ES Analysis

In this section, the allocation of ESs as well as the behavior of the calendering machine are discussed. In **Figure 4**, the division of the ESs by the compaction stages of the calendering process is shown. Each individual DMC as ES identifier represented a single data point, which was assigned to the respective ES. For clarity, it should be noted that only the respective start and end ES identifier are shown on the *x*-axis, which delineates an ES. For the subsequent analyses, ES 1, which features the highest rolling force set at 350 kN, is designated as the most calendered, while ES 7 corresponds to the non calendered electrode. Between the individual compaction stages, the DMCs of the ESs were not assigned to any ES due to the necessity of setting the rolling force for the calendering machine within this segment. As demonstrated in Figure 4, the calendering machine applied a constant rolling force for the length of each compression stage during the processing of the electrode coil, which facilitated the clear assignment of the DMCs to the ESs on the basis of the different rolling forces.

Furthermore, it is evident that the compaction stages vary in length, attributable to the assignment of a differing number of electrode markings to each ES. The quality of some DMCs was found to be inadequate, resulting in their undetectability by the code reader within the calendering machine. It was observed that the length of each compaction stage was maintained at ≈8 m, with a constant web speed of 1 m min^{-1}, allowing for a permissible deviation of a few (centi-)meters.

Since a constant rolling force was applied during processing at each compaction stage, it could be assumed that the reduction of the electrode thickness was homogeneous along an ES. Therefore, the measured inline and offline data of the electrodes studied within an ES were averaged for further evaluation, as any variations in the measurements were considered negligible.

During the calendering process of each ES, the roll gap between the upper and lower roll was measured with the capacitive sensors on the left and right in parallel. The behavior of the particular calendering machine is of crucial importance for process understanding, as the machine-specific behavior and process parameters have a direct influence on the electrode properties that are achieved. In **Figure 5**, the measured roll gap and its standard deviation for every ES are shown over the respective measured rolling force for the EA 102 calendering system at *iwb*. The data for ES 7 (0 kN) is not shown because of the opened roll gap. In this case, the measuring technique no longer detects a viable roll gap value.

The roll gap of the EA 102 calendering machine behaves approximately linearly with the measured rolling force. As the latter increased, the roll gap decreased, and consequently, the electrode experienced a greater degree of compaction. For ES 6, the mean measured roll gap was at around 120 µm, while for ES 1, the mean roll gap was measured to be at around 65 µm. The linear shape is in agreement with the analyses conducted by Diener et al.,[31] which established a direct correlation between the decrease in roll gap in a direct roll gap measurement and the applied compaction degree. It is important to note that the machines used in this study are not identical and that different mechanical behaviors may occur during the process. Calendering systems from different manufacturers exhibit different rollers displacements due to varying machine stiffnesses and bearings.[11] Furthermore, the composition of the electrode and the mass loading, as input product characteristics, influence the product behavior in the measured roll gap.[31] The comparatively linear relationship can be utilized for future switch-on

Research Article
doi.org/10.1002/batt.202500133
Chemistry Europe
European Chemical Societies Publishing

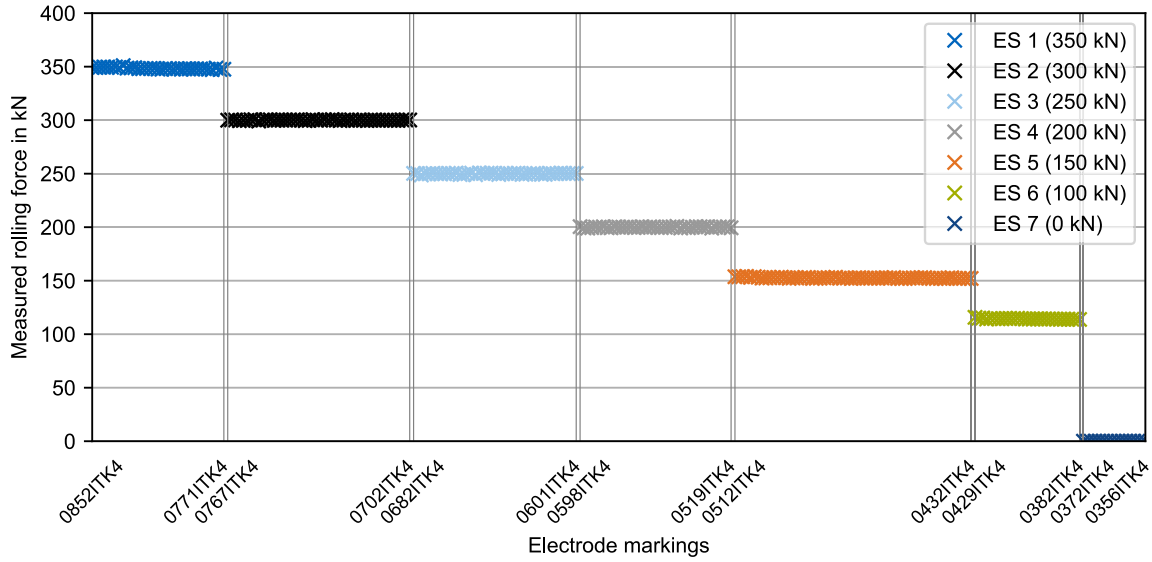

Figure 4. Illustration of the division of electrode markings into their respective ES. Each compaction stage and the corresponding target value for the rolling force between 350 and 0 kN defines an ES.

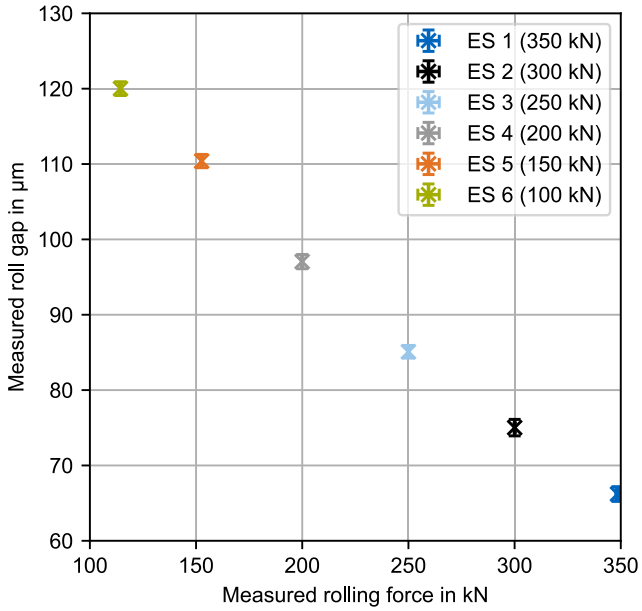

Figure 5. Measured roll gap of the calendering machine in relation to the measured rolling force of the ESs.

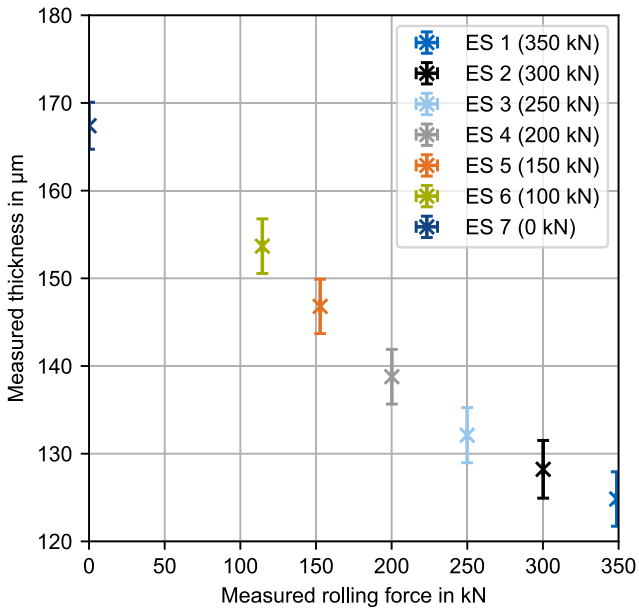

Figure 6. Measured thickness of the electrode samples from the respective ESs at the associated rolling forces.

processes to derive the roll gap as a function of the rolling force with high accuracy within the framework of machine- and material-specific applications. This is enabled by the highly granular resolution of the traceability system and the systematic stepwise compression, which characterizes the deformation behavior of the electrode during the calendering process in a specific parameter range, as presented in this study.

4.2. Process Product Interactions

In this section, the influence of the set process parameters on the measured inline and offline data is discussed. Based on the findings of Figure 5, the resulting thickness of the electrode was investigated. In **Figure 6**, the measured electrode thickness is shown in relation to the rolling force.

The measured electrode thickness of ≈167 µm at 0 kN corresponded to the initial thickness in the non calendered state. With an increase in calendering degree, a decrease in electrode thickness was recorded until a minimum of ≈125 µm at the 350 kN of rolling force was attained. In contrast to the measured linear relationship shown in Figure 5, a weakening decrease in electrode thickness was evident with increasing rolling force. As the compaction rate increases, the material-intrinsic compaction resistance rises, particularly in the case of NMC622 cathodes.

This is due to the hardness of the NMC622 particles and the associated increased friction within the coating. Accordingly, NMC particles require higher rolling forces for particle–particle rearrangement or particle deformation. As a result, a gradual convergence to a minimal thickness, respectively minimal porosity, becomes apparent.[12,42]

The commercial electrode used in this study had a consistently higher mass loading in the middle of the electrode web, which led to a comparatively higher thickness in the middle section compared to the sides and explains the slightly increased standard deviation seen in Figure 6. These findings were supported by the measurement of the three sample positions regarding electrode mass and thickness (see Figure S1 and S2, Supporting Information). The process tolerance of the electrode thickness achieved during calendering is of particular importance in terms of homogeneity. Deviations from set target values can result in variations in porosity, thereby impacting the electrochemical performance of the final LIB.[43]

The achieved porosity was determined using the gas pycnometer. Additionally, the ratio of the bulk volume of the electrode components to the volume of the coating was used to calculate the porosity of the electrode coating, based on the thickness measurement with the gauge.[14] In **Figure 7**, the different calculated porosities of the ESs are given.

It can be observed that the electrode in the non calendered state had an initial porosity of ≈46%. As the calendering degree increases, the porosity decreases to a minimum value of ≈25% at 350 kN. Furthermore, the gauge-based calculated porosity tends to show higher values compared to the pycnometer. Due to the different measuring points for thickness at the various sample positions, the method based on the gauge shows deviations, whereas the pycnometer measurement provides a scalar value for each ES based on the described measurement principle.

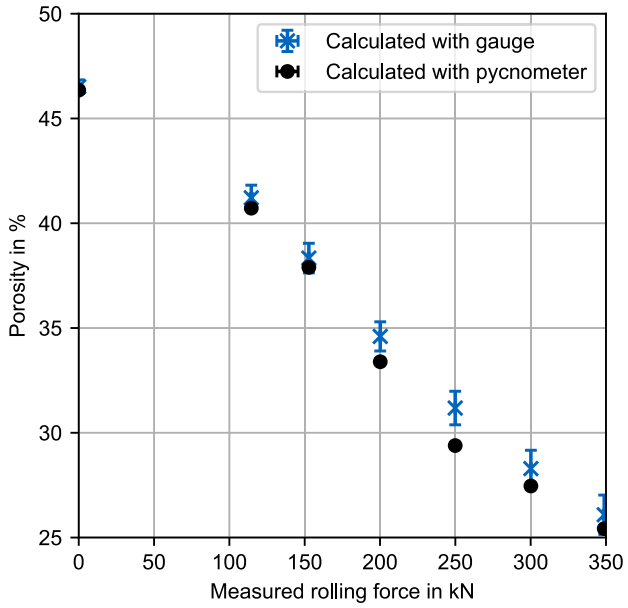

Figure 7. Calculated electrode porosity based on the measurements with the gauge and the pycnometer from the respective ESs at the associated rolling forces.

The discrepancy between the two analytical methods can be ascribed to closed pores in the coating matrix that are inaccessible to the gas pycnometer. Such closed pores may be present, for instance, in the secondary particles of the active material or between agglomerates of conductive additives. Furthermore, it should be emphasized that a deviation of ≈2% in porosity cannot be considered significant for the analytical methods utilized, for example, due to the measurement tolerance of tactile thickness measurement.[44] Similar to the trend of decreasing electrode thickness with increasing rolling forces, the porosity also decreases gradually to a minimum, though less significantly at higher compaction levels. This behavior has already been explained in the previous section.

A comprehensive understanding of the correlation between the process and electrode structure, manifesting as quality-limiting defect patterns, is critical for achieving objectives related to enhanced compression rates and minimized porosity levels. Increases in the rolling force, for instance, have been shown to induce electrode corrugation.[3,24] To illustrate the increase in the defect pattern as a result of compaction, **Figure 8**a shows a section of the monochromatic images from the laser triangulation sensors. In Figure 8b, the quantified DEI values for the respective ESs are displayed.

As seen in Figure 8a, the electrode corrugation was strongest at the highest compaction level in ES 1 and decreased with declining rolling force, until almost no visible corrugation was observed in ES 6 respectively ES 7. The corrugation is evident across the entire width of the electrode, with a superimposition of smaller corrugations being visible at the edge of the coating. This observation aligns with previous analyses of the defect pattern of the electrode corrugation.[24] The decrease in electrode corrugations is also quantitatively observed in the DEI value. As demonstrated in Figure 8b, the progression of the DEI values is characterized by a linear trend with increasing compression rate, which is consistent with the findings of comparable investigations regarding corrugation intensity.[24,29,30] In ES 1, the highest mean DEI was determined at ≈4.8 mm, while the lightest calendered section, ES 6, was at ≈1.6 mm. In the non calendered state, the lowest mean DEI of ≈0.9 mm was detected. The DEI value in this section was not 0 because there was slight vibration in the roll-to-roll web guide caused by the open roll gap and a longer section without roll engagement, resulting in less stable web guidance. The analysis of the electrode corrugation indicates that this phenomenon occurs as a consequence of intense calendering. The electrode corrugation is formed by the plastic stretching of the coating in the longitudinal and transverse directions of the electrode, although the stretching transverse to the process direction is less pronounced.[45] Mayer et al.[45] demonstrated that the disparity in length between the coated areas and the uncoated substrate foil is of particular significance for the formation of the electrode corrugation. During the compaction process, only the coating is in contact with the rollers and undergoes elongation, whereas the uncoated substrate foil remains unaffected. The varying interaction of the individual segments with the rolls leads to the development of residual stresses in the electrode web. At a low compaction rate, no corrugation was observed on electrodes where the uncoated substrate foil had been removed

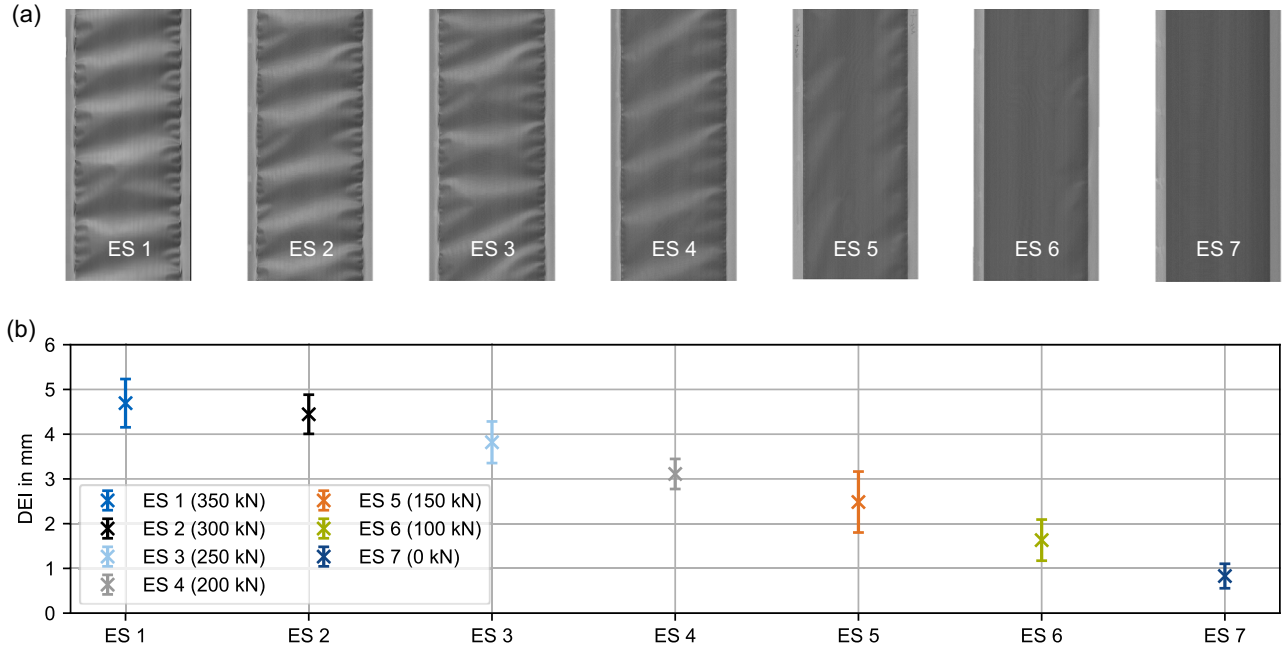

Figure 8. Excerpts of sensor recordings of the electrodes from the various ESs in (a) and quantitative DEI evaluation of the ES in (b). The visible corrugation of the electrodes is quantitatively described using the DEI.

at the edge.[45] The elongation in the process direction depends not only on the set process parameters but also on the roll diameter of the calendering machine, with the percentage elongation decreasing with larger roll diameters.[46] The intensity of the electrode corrugation can be affected by an inhomogeneous density distribution within the electrode coating, which can result from an inhomogeneous electrode thickness from the upstream process steps of coating and drying.[3] This was also observed in the commercial NMC622 cathode in the present study (see Figure S1 and S2 Supporting Information).

The traceability system allowed for a clear assignment of the corrugation characteristics to individual DMCs and consequently to individual ESs, as the markings applied to the electrode were recognizable via the image recordings. The corrugations of the electrodes presented in Figure 8 have a negative effect on subsequent process steps, including the stacking of the separated electrode sheets.[3,30] Increasing the roll temperature has been shown to reduce the rolling forces required for compaction at higher roll temperatures,[18] thus improving processability and reducing calendering-induced defects and scrap.[14,24,29] Consequently, inline quantification employing laser triangulation and the DEI provides significant insights into the relationships between process and the electrode structure and can be clearly traced back to set process parameters in conjunction with the traceability system.

The microstructural deformations that occur in the electrode coating during calendering exert a significant influence on the quality of the electrode. This is evident in the form of geometric defect patterns like electrode corrugations as seen in Figure 8a and also extends to the interface with the substrate foil. The presence of particle indentations at the interface between the coating and the substrate foil has been demonstrated to exert a significant influence on the electrical[47] and thermal conductivity,[19,47] as well as the adhesion strength.[11] To ensure the effective parameterization of the calendering process, it is crucial that the process–structure relationship between the particle indentations in the substrate foil and the resulting quality characteristics of the electrode is thoroughly investigated. The qualitative LSM images and the quantification of the particle indentations in the substrate foil after calendering of each ES are depicted in **Figure 9**.

The LSM images in Figure 9a clearly show an increase in particle indentations with increasing compaction. In ES 7, the decoated substrate foil showed only minimal indentations and scratches. These may have originated from the decoating process or from the rolling process used to manufacture the aluminum substrate foil. At low compaction levels in ES 6 and ES 5, the first individual particle indentations were visible. As expected, the most pronounced microstructural deformations were found in the strongly calendered electrodes from ES 2 and ES 1. The phenomenon of active material particles embedded in an aluminum substrate foil as a result of increased calendering has already been observed in different studies investigating the typical active materials NMC[11,19,47,48] and lithium ferro-phosphate (LFP).[49]

To the best of the authors' knowledge, the deformations at the interface resulting from the particle indentations have so far only been considered qualitatively, or in individual cases the surface roughness of the substrate foil has been analyzed,[20,50] but not the specific number of indentations caused by active material particles. Figure 9b displays the corresponding quantification of the particle indentations for the respective ESs. In ES 7, as a non calendered reference, a low average number of fewer than 50 particle indentations was measured. These can be attributed to manufacturing-related dents or small scratches, as previously

Research Article
doi.org/10.1002/batt.202500133
Chemistry Europe
European Chemical Societies Publishing

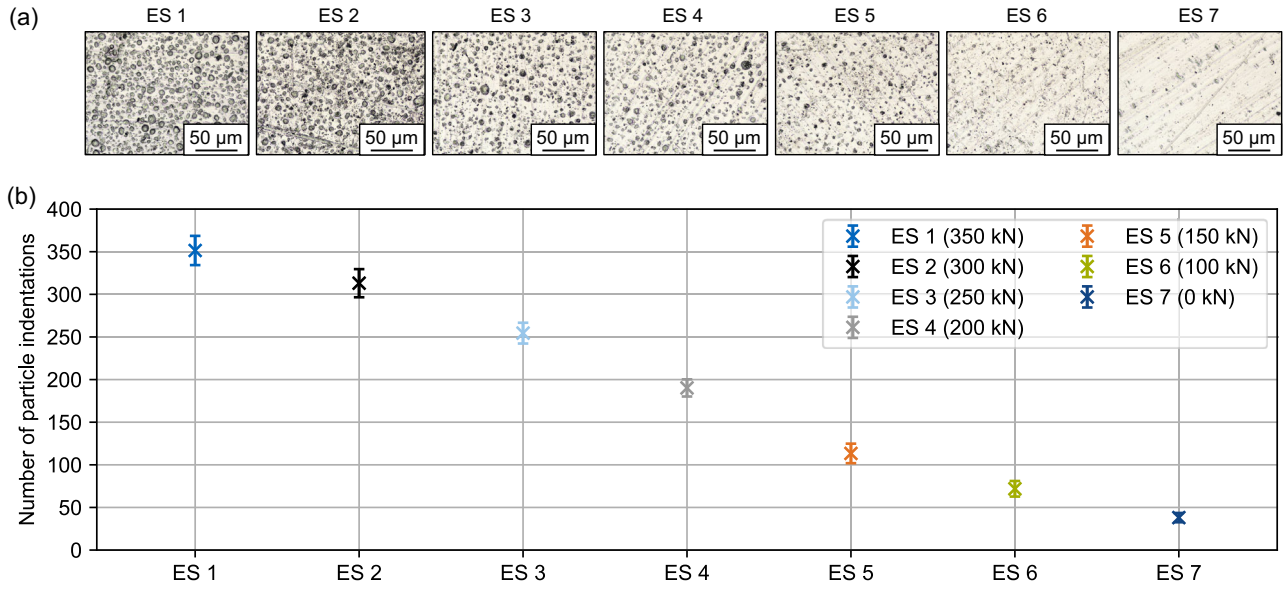

Figure 9. Representation of the microstructural deformation in the substrate foil in the form of particle indentations based on exemplary LSM images in (a) and quantification of the number of particle indentations for each ES in (b).

mentioned. As the degree of compaction increases, the number of particle indentations increases linearly, reaching a maximum of ≈350 particle indentations on average for ES 1 and its specific electrode samples. An increase in the particle indentations, and the associated increase in the contact area between the active material particles and the substrate foil, has been demonstrated to influence thermal conductivity.[19,20] Gandert et al.[19] found that the effective thermal conductivity is also improved with the increasing embedding of the particles in the substrate foil. Consequently, the thermal contact resistance at the interface between the coating and the substrate foil exerts an influence on the thermal conductivity at the electrode stack level.[19] The enhancement of heat transport resulting from the mechanical interlocking of the active material particles in the substrate foil was also identified by Zhang et al. and was the subject of further investigation in simulation studies.[20,47] The number of contact points at the interface, as determined by means of simulation,[20] is of a similar order of magnitude to the experimentally quantified particle indentations in this study. The methodology presented in this work therefore offers the opportunity to validate the simulation results and gain further insights into process–structure relationships at the interface.

In addition to the effect on thermal conductivity, the electrical contact resistance respectively the electrical conductivity at the interface to the substrate foil are influenced by the particle indentations. In the context of this study, the interfacial resistance was determined experimentally for the ESs accordingly. The correlation between the interfacial resistance and the measured rolling force is illustrated in **Figure 10**.

In the non calendered state, the electrode exhibited the highest interfacial resistance with ≈0.32 Ω cm^2. With increasing rolling force, the resistance decreased, reaching a minimum value of 0.02 Ω cm^2 for the investigated process parameters. The reduction in interfacial resistance is directly correlated with the increase

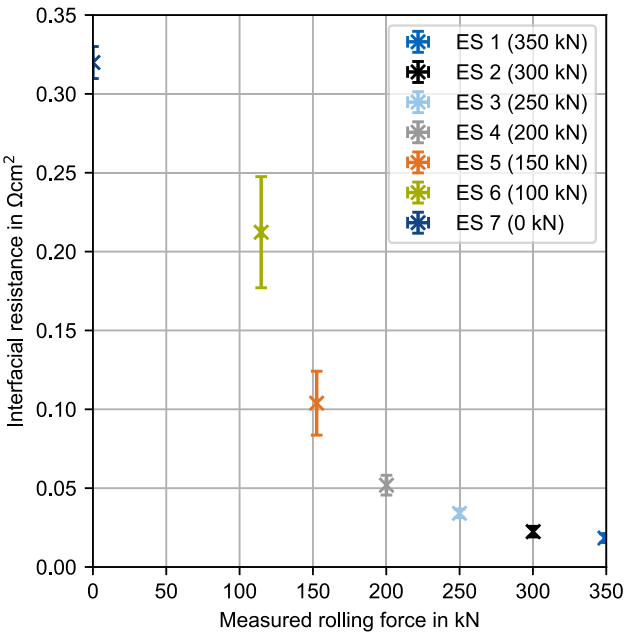

Figure 10. Measured interfacial resistance at the interface between substrate foil and coating matrix of the ESs at the associated rolling forces.

in the number of particle indentations at elevated compaction levels, resulting in an enhancement of the contact area with the substrate foil. The curve shape is consistent with the results available in the literature.[47] However, it should be noted that the absolute values are different as a result of differences in the material systems and measurement methods. Van Bommel et al.[49] observed a comparable development of the contact resistance at the interface for LFP cathodes, as determined by electrochemical impedance spectroscopy analysis. The reduced impedance of the calendered electrodes was mainly caused by the penetration

of the LFP particles into the substrate foil. This resulted in a better discharge rate capability for the LFP cathodes investigated due to lower overpotentials.[49]

Furthermore, the particle indentations influence the mechanical quality parameters of the electrode, with the mechanical interlocking influencing the form stability of the substrate foil for the processing in roll-to-roll processes. Excessive calendering and the resulting deformations can lead to thinning in the substrate foil. This results in reduced tensile strength and the formation of weak points, which can lead to the development of foil tears and, consequently, scrap.[20,50]

As previously indicated, another key quality parameter for the electrode is the adhesion strength between the substrate foil and the coating. The investigation of the adhesion strength development for the process parameters examined in this study is presented in **Figure 11**.

As demonstrated in Figure 11, the adhesion strength exhibits a distinctive U-shaped curve in relation to the degree of compaction. Initially, the adhesion strength declines to a minimum, starting from the non calendered reference state and subsequently increases again. In this study, the minimum was reached in ES 4 at 200 kN rolling force, respectively, a correlating porosity between 30% and 35% (see Figure 7). This finding is consistent with the porosity values reported in the literature for cathodes.[11,18] It is important to note that the differences in terms of the absolute values for the adhesion strength and the slope of the curve are due to existing dependencies on the product properties, for example, active material and mass loading, but the shape of the curve is comparable to previous findings. The initial decrease in adhesion strength can be attributed to the shear and normal stresses prevailing on the electrode in the roll gap during calendering. This results in a high stress at the interface between the coating matrix and the substrate foil, which in turn weakens the bonds set by the preceding process steps at the interface.[18,48] As previously stated, the increase in adhesion strength for a stronger compaction after reaching the minimum is explained by the indentation of the active material particles into the substrate foil, which leads to an increased contact area and thus mechanical interlocking.[18,48,51] These findings emphasize the significance of the process–structure relationship at the interface in terms of electrode quality, thus necessitating a tradeoff between electrochemical properties and interface bonding for an efficient parameterization of the calendering process.[20] The quantification of the number of particle indentations as an index for the contact area used in this study allows for a more detailed description of the microstructural deformations in the substrate foil. In combination with the traceability system, it is possible to systematically identify quality-relevant process–structure relationships with a manageable amount of experimental effort and electrode material. Furthermore, the effects of process fluctuations on the product parameters can be analyzed for different machine settings.

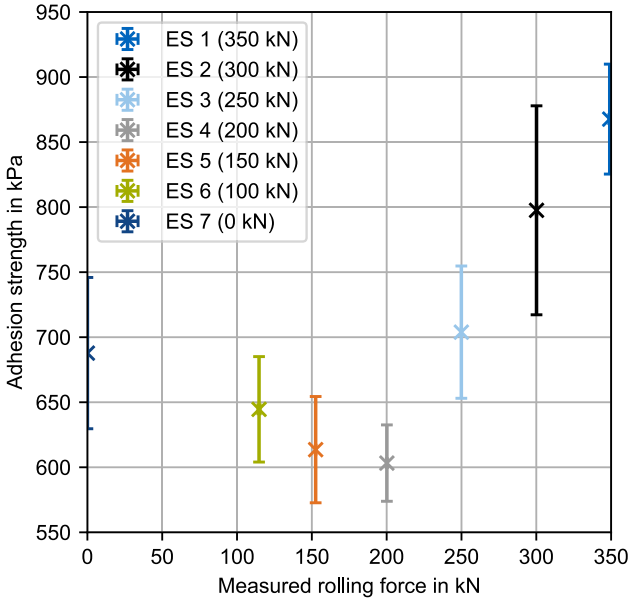

Figure 11. Measured adhesion strength at the interface between substrate foil and coating matrix of the ESs at the associated rolling forces.

5. Conclusion

This work aimed to describe the compaction behavior of an electrode and its effects on quality-relevant product properties using a marker-based traceability system. A commercially procured electrode was marked with a laser marking system in the *iwb* coating machine. The electrode was calendered in steps of increasing rolling force, with inline measurement data assigned to specific ESs using the traceability system. After calendering, offline measurements of electrode thickness, particle indentations, porosity, interfacial resistance, and adhesion strength were performed and linked to the corresponding ESs. The connection between offline measurement data and inline production parameters was established systematically through the markings on the substrate foil, allowing for quality-relevant correlations between production data to be derived.

In the course of the calendering process, the gap between the rollers was measured in this study. This revealed an approximately linear relationship between the rolling force of the calendering machine and the size of the gap. As the rolling force increased, the gap decreased, resulting in more densely compacted electrodes. This linear behavior allows the roll gap to be accurately calculated from the rolling force for a given material and machine in the future. This will reduce the need to adjust process parameters during startup.

The DEI was used to quantify the corrugation and assess the processability of the electrode and showed a linear increase with increasing compaction. This quantitative measurement of electrode corrugations allowed defects to be traced back to specific process parameters, highlighting the importance of avoiding excessive corrugations for better electrode processability. The microstructural deformations at the interface with the substrate foil exerted a direct influence on the quality of the electrode. This influence was measured using an advanced method that determined the number of particle indentations. With increasing compaction, the number of particle indentations increased, accompanied by a reduction in electrical contact resistance

and an improvement in adhesive strength due to mechanical interlocking.

The traceability system was used to demonstrate the relationship between the machine parameters and resulting product properties, and local anomalies in the form of defect patterns on a highly granular scale. This was achieved using both qualitative and quantitative methods. The systematic combination of inline and offline data enables a holistic characterization of the compaction behavior of the electrode, thus facilitating the derivation of process parameters depending on targeted product parameters.

The gradual compaction of an electrode in combination with the automated tracking and tracing of inline parameters offers the potential to characterize new material systems in a short section with regard to compaction behavior. This approach has the potential to considerably minimize the effort required for subsequent process startups.

In future work, the methodology for analyzing the particle indentations will be extended by calculating the contact area based on the number, the depth, and the diameter of the detected indentations. In terms of the product, the influence of the substrate foil will also be investigated in relation to the process–structure relationships, given the significant impact of thickness and degree of hardness of the aluminum foil on the deformations occurring at the interface.

Acknowledgements

The authors express their gratitude toward the Federal Ministry of Education and Research (BMBF) for funding the research. The presented content in this article has been achieved within the scope of the projects "InteKal" (FKZ: 03XP0348B) and "TrackBatt" (FKZ: 03XP0310A). Furthermore, the authors would like to thank their research partners and project coordinator Juelich for their trustful cooperation and support within the project. Additionally, gratitude is extended to Felix Weißenburger and Yunhao Liang for their assistance in conducting the measurements. Many thanks to Sophie Grabmann for her assistance in proofreading.

Open Access funding enabled and organized by Projekt DEAL.

Conflict of Interest

The authors declare no conflict of interest.

Author Contributions

Andreas Mayr: conceptualization (lead); data curation (equal); formal analysis (equal); investigation (lead); methodology (equal); software (supporting); validation (equal); visualization (equal); writing—original draft (lead); and writing—review and editing (lead). **Alessandro Sommer**: conceptualization (equal); data curation (equal); formal analysis (lead); investigation (equal); methodology (equal); software (lead); validation (equal); visualization (equal); writing—original draft (equal); and writing—review and editing: (equal). **Julian Link**: formal analysis (supporting); investigation (supporting); visualization (supporting); and writing—original draft (supporting). **Johannes Schachtl**: investigation (supporting) and writing—original draft (supporting). **Rüdiger Daub**: funding acquisition: (lead); supervision (lead); writing—original draft (supporting); and writing—review and editing: (supporting). Andreas Mayr and Alessandro Sommer contributed equally to this work.

Data Availability Statement

The data that support the findings of this study are available from the corresponding author upon reasonable request.

Keywords: calendering · electrode production · lithium-ion batteries · tracking and tracing

[1] F. Duffner, L. Mauler, M. Wentker, J. Leker, M. Winter, *Int. J. Prod. Econ.* **2021**, *232*, 107982.
[2] A. Kwade, W. Haselrieder, R. Leithoff, A. Modlinger, F. Dietrich, K. Droeder, *Nat. Energy* **2018**, *3*, 290.
[3] T. Günther, D. Schreiner, A. Metkar, C. Meyer, A. Kwade, G. Reinhart, *Energy Technol.* **2020**, *8*, 1900026.
[4] M. Westermeier, G. Reinhart, M. Steber, *Proc. CIRP* **2014**, *20*, 13.
[5] L. Mauler, F. Duffner, W. G. Zeier, J. Leker, *Energy Environ. Sci.* **2021**, *14*, 4712.
[6] L. Mauler, F. Duffner, J. Leker, *Appl. Energy* **2021**, *286*, 116499.
[7] M. Winter, R. J. Brodd, *Chem. Rev.* **2004**, *104*, 4245.
[8] T. Günther, N. Billot, J. Schuster, J. Schnell, F. B. Spingler, H. A. Gasteiger, *AMR* **2016**, *1140*, 304.
[9] M. Keppeler, S. Roessler, W. Braunwarth, *Energy Technol.* **2020**, *8*, 2000183.
[10] M. Kehrer, M. Locke, C. Offermanns, H. Heimes, A. Kampker, *Energy Technol.* **2021**, *9*, 2001113.
[11] D. Schreiner, M. Oguntke, T. Günther, G. Reinhart, *Energy Technol.* **2019**, *7*, 1900840.
[12] C. Meyer, H. Bockholt, W. Haselrieder, A. Kwade, *J. Mater. Process. Technol.* **2017**, *249*, 172.
[13] H. Zheng, L. Tan, G. Liu, X. Song, V. S. Battaglia, *J. Power Sources* **2012**, *208*, 52.
[14] D. Schreiner, T. Zünd, F. J. Günter, L. Kraft, B. Stumper, F. Linsenmann, M. Schüßler, R. Wilhelm, A. Jossen, G. Reinhart, et al., *J. Electrochem. Soc.* **2021**, *168*, 30507.
[15] M. Abdollahifar, H. Cavers, S. Scheffler, A. Diener, M. Lippke, A. Kwade, *Adv. Energy Mater.* **2023**, *13*, 2300973.
[16] Y.-H. Chen, C.-W. Wang, X. Zhang, A. M. Sastry, *J. Power Sources* **2010**, *195*, 2851.
[17] W. Haselrieder, S. Ivanov, D. K. Christen, H. Bockholt, A. Kwade, *ECS Trans.* **2013**, *50*, 59.
[18] C. Meyer, M. Weyhe, W. Haselrieder, A. Kwade, *Energy Technol.* **2020**, *8*, 1900175.
[19] J. C. Gandert, M. Müller, S. Paarmann, O. Queisser, T. Wetzel, *Energy Technol.* **2023**, *11*, 2300259.
[20] J. Zhang, J. Sun, H. Huang, Z. Yuan, *Particuology* **2024**, *85*, 252.
[21] D. Schreiner, J. Lindenblatt, R. Daub, G. Reinhart, *Energy Technol.* **2023**, *11*, 2200442.
[22] N. Billot, T. Günther, D. Schreiner, R. Stahl, J. Kranner, M. Beyer, G. Reinhart, *Energy Technol.* **2020**, *8*, 1801136.
[23] C. Schilcher, C. Meyer, A. Kwade, *Energy Technol.* **2016**, *4*, 1604.
[24] A. Mayr, D. Schreiner, B. Stumper, R. Daub, *Proc. CIRP* **2022**, *107*, 295.
[25] A.-K. Wurba, V. Bauer, K. Seiraffi, J. Fleischer, *Proc. CIRP* **2024**, *130*, 456.
[26] H.-Y. Tran, A. Lindner, W. Menesklou, W. Braunwarth, *Energy Technol.* **2023**, *11*, 2201092.
[27] S. Haghi, M. Leeb, A. Molzberger, R. Daub, *Energy Technol.* **2023**, *11*, 2300364.
[28] A.-K. Wurba, J. Klemens, D. Mayer, C. Reusch, L. Altmann, O. Leonet, J. A. Blázquez, I. Boyano, E. Ayerbe, P. Scharfer, et al., *Proc. CIRP* **2023**, *120*, 314.

[29] A.-K. Wurba, L. Altmann, J. Fleischer, *Prod. Eng. Res. Dev.* **2024**, *18*, 497.
[30] D. Mayer, B. Schwab, J. Fleischer, *Energy Technol.* **2023**, *11*, 2200870.
[31] A. Diener, S. Ivanov, W. Haselrieder, A. Kwade, *Energy Technol.* **2022**, *10*, 2101033.
[32] A. Sommer, M. Leeb, S. Haghi, F. J. Günter, G. Reinhart, *Proc. CIRP* **2021**, *104*, 1011.
[33] A. Sommer, S. Bazlen, H.-Y. Tran, M. Leeb, J. Wachter, W. Braunwarth, R. Daub, *Energy Technol.* **2024**, *12*, 2301221.
[34] M. F. Niri, K. Liu, G. Apachitei, L. A. Román-Ramírez, M. Lain, D. Widanage, J. Marco, *Energy AI* **2022**, *7*, 100129.
[35] S. Haghi, Y. Chen, A. Molzberger, R. Daub, *Batter. Supercaps* **2024**, 7.
[36] G. Riexinger, J. P. Doppler, C. Haar, M. Trierweiler, A. Buss, K. Schöbel, D. Ensling, T. Bauernhansl, *Proc. CIRP* **2020**, *93*, 125.
[37] A. Sommer, J. Wachter, S. Grabmann, R. Daub, *Batter. Supercaps* **2024**, 7.
[38] A. Sommer, M. Leeb, L. Weishaeupl, R. Daub, *Batteries* **2023**, *9*, 89.
[39] A. Sommer, S. Bazlen, H.-Y. Tran, W. Braunwarth, R. Daub, *Proc. CIRP* **2023**, *120*, 171.
[40] W. Haselrieder, B. Westphal, H. Bockholt, A. Diener, S. Höft, A. Kwade, *Int. J. Adhes. Adhes.* **2015**, *60*, 1.
[41] L. Hille, P. Hoffmann, J. Kriegler, A. Mayr, M. F. Zaeh, *Prod. Eng. Res. Dev.* **2023**, *17*, 773.
[42] C. Meyer, M. Kosfeld, W. Haselrieder, A. Kwade, *J. Energy Storage* **2018**, *18*, 371.
[43] W. Yourey, *Batteries* **2020**, *6*, 23.
[44] T. Beuse, M. Fingerle, C. Wagner, M. Winter, M. Börner, *Batteries* **2021**, *7*, 70.
[45] D. Mayer, A.-K. Wurba, B. Bold, J. Bernecker, A. Smith, J. Fleischer, *Processes* **2021**, *9*, 2009.
[46] D. Wang, G. Wang, C. Xu, H. Liu, *J. Energy Storage* **2024**, *87*, 111521.
[47] J. Zhang, H. Huang, J. Sun, *Powder Technol.* **2022**, *409*, 117828.
[48] W. Haselrieder, *Dissertation*, Technische Universität Braunschweig; Sierke Verlag.
[49] A. van Bommel, R. Divigalpitiya, *J. Electrochem. Soc.* **2012**, *159*, A1791.
[50] J. Zhang, J. Sun, H. Huang, C. Ji, M. Yan, Z. Yuan, *Appl. Energy* **2024**, *373*, 123900.
[51] H. Y. Tran, G. Greco, C. Täubert, M. Wohlfahrt-Mehrens, W. Haselrieder, A. Kwade, *J. Power Sources* **2012**, *210*, 276.

Manuscript received: February 25, 2025
Revised manuscript received: March 11, 2025
Version of record online: March 17, 2025